Journal of Magnetism and Magnetic Materials 499 (2020) 166189

Contents lists available at ScienceDirect

Journal of Magnetism and Magnetic Materials

journal homepage: www.elsevier.com/locate/jmmm

Research articles

Thermoeconomic performance optimization of an irreversible Brayton refrigeration cycle using Gd, $Gd_{0.95}Dy_{0.05}$ or $Gd_{0.95}Er_{0.05}$ as the working substance

Zhimin Yang[a,b,1], Zhichao Xu[c,1], Junyi Wang[d,*], Yan Li[a], Guoxing Lin[a,*], Jincan Chen[a]

[a] Department of Physics, Xiamen University, Xiamen 361005, China
[b] School of Physics and Electronic Information, Yan'an University, Yan'an 716000, China
[c] Ministry of Education's Key Laboratory of Poyang Lake Wetland and Watershed Research, Jiangxi, Normal University, Nanchang 330022, China
[d] Department of Physics, Jimei University, Xiamen 361021, China

ARTICLE INFO

Keywords:
Magnetocaloric material
Refrigeration cycle
Thermoeconomic performance
Irreversible loss
Optimization

ABSTRACT

An irreversible regenerative Brayton refrigerator cycle is established, in which the nonperfect regenerator, regenerative time, heat leak, and irreversible adiabatic processes are taken into account. The mathematical expressions of the refrigeration rate, coefficient of performance, and thermoeconomic function of the refrigeration cycle are derived and the thermoeconomic function is optimized. Moreover, choosing Gd, $Gd_{0.95}Dy_{0.05}$ and $Gd_{0.95}Er_{0.05}$ as the working substances respectively, we discussed in detail the influences of the thermoeconomic and thermodynamic parameters on the optimal thermoeconomic and thermodynamic performances. The results show that the thermoeconomic performance of the refrigeration cycle using Gd or $Gd_{0.95}Dy_{0.05}$ as the working substance is better than that using $Gd_{0.95}Er_{0.05}$ and the thermoeconomic performance of the refrigeration cycle using $Gd_{0.95}Dy_{0.05}$ as the working substance is better than that using Gd in the situation with the lower adiabatic magnetization.

1. Introduction

Magnetic refrigeration [1–8] based on MCE is one of the green refrigeration technologies and has attracted more and more attention. Due to its high efficiency (reach up to 60% of the Carnot efficiency), environment-friendly, structure compactness, without noise, and save energy [9], magnetic refrigeration is regarded as a promising alternative to traditional refrigeration technology.

Considerable efforts have been made to promote the development of magnetic materials and magnetic refrigerators. Gadolinium (Gd) with the Curie temperature of 293 K is considered to be an ideal working substance for room temperature magnetic refrigerators and has been efficiently utilized in current prototypes. Even it is often thought as a reference material for comparing purpose. A magnetic refrigerator requires a large temperature span and constant magnetic entropy as a function of temperature [10]. Relatively to Gd, Gd-based alloys such as gadolinium-dysprosium (Gd-Dy), gadolinium-erbium (Gd-Er), and gadolinium-Terbium (Gd-Tb) can be used as the working substances to shift the Curie temperature [11]. MCE can be enhanced with high magnetic fields and therefore the MCE of some magnetocaloric materials in high steady magnetic fields were studied by direct measurements of the adiabatic temperature change [12,13]. Furthermore, a number of researchers have explored some MCE materials such as $Gd_5(Si_2Ge_2)$ and La-Fe-Si- and Mn-Fe-P-based alloys. Pecharsky et al. [14] discovered an extremely large magnetic entropy change in $Gd_5(Si_2Ge_2)$ when it was subjected to a change in the magnetic field. Aprea et al. [15] compared the performance of $Gd_5(Si_2Ge_2)$, $Fe_{11.384}Mn_{0.356}Si_{1.26}H_{1.52}$, $LaFe_{11.05}Co_{0.94}Si_{1.10}$, $MnFeP_{0.45}As_{0.55}$, and $Pr_{0.65}Sr_{0.35}MnO_3$ with that of Gd and found that $Gd_5(Si_2Ge_2)$ is the best candidate to magnetic refrigeration due to its large temperature span and *COP*. Although Mn-Fe-P- and La-Fe-Si-based alloys are first-order materials, some of them are also promising ones for room-temperature application, because the thermal hysteresis may be adjusted to small enough and the entropy change values can reach 16.5 J kg^{-1} K^{-1} and 14.8 J kg^{-1} K^{-1} for Mn-Fe-P- and La-Fe-Si-based alloys compared with 5.6 J kg^{-1} K^{-1} of Gd [16]. Franco et al. [17] analyzed different magnetocaloric materials, such as Gd and Gd-based alloy, La-Fe-Si-based alloy, Gd-Si-Ge-based alloy, and Ferromagnetic Lanthanum Manganites,

* Corresponding authors.
E-mail addresses: jywang@jmu.edu.cn (J. Wang), gxlin@xmu.edu.cn (G. Lin).
[1] The two authors contribute equally to this work.

https://doi.org/10.1016/j.jmmm.2019.166189
Received 6 June 2019; Received in revised form 18 October 2019; Accepted 20 November 2019
Available online 30 November 2019
0304-8853/

Nomenclature

A	area of heat exchange, m^2
a	cost per unit heat exchanger area, ncu/(year, m^2)
B_J	Brillouin function,
b	cost per unit power input, ncu/(year, w)
C	heat capacity, J/(Kg K)
C_e	energy cost, ncu/year
C_i	investment cost, ncu/year
F	thermoeconomic function
g	Lande factor
H	applied magnetic field, T
I_{leak}	dimensionless heat leak coefficient
J	quantum number of angular momentum
k	thermoeconomic parameter
k'	Boltzmann constant, J/K
M	magnetization, Am^2/kg
M_m	molar mass, kg/mol
N	number of magnetic moment
ncu	national currency unit
P	power input, w
Q	exchanged heat, J
Q_{net}	net cooling quantity, J
ΔQ_r	additional regenerative loss, J
R	cooling rate, w
R'	universal gas constant, J/(mol K)
R^*	dimensionless cooling rate
T	temperature, K
t	heat exchange time, s
t_r	time of two regenerative processes, s
U	heat transfer or heat leak coefficient, $J/(m^2K)$
u	percentage of magnetic material's price in magnetic refrigerator
W	work input, J

Greek letter

β	area distribution of heat exchanger
η	regenerator efficiency
η_{mag}	irreversible adiabatic magnetization factor
η_{demag}	irreversible adiabatic demagnetization factor
λ'	molecular field coefficient
μ_0	permeability of vacuum, F/m
μ_B	Bohr magneton, eV/T
ρ	mass density, kg/m^3

Subscript

a, b, b', c, d, e, e', f	state point
h	high temperature side
l	low temperature side
leak	heat leak
r	regenerator

abbreviation

COP	coefficient of performance
MCE	magnetocaloric effect

and possible routes to improve their performance. Samanta et al. [18] observed a giant MCE in $ErRu_2Si_2$ when field-induced metamagnetic transmits from an antiferromagnetic to a ferromagnetic state. Guo et al. [19] observed that the magnetic entropy change in the polycrystalline of $La_{1-x}Ca_xMnO_3$ (x = 0.2 and 0.33) perovskite-type manganese oxide is larger than that in Gd. On the other hand, some prototype machines have also been designed, built, and tested. Gómez et al. [20] presented a reciprocating room temperature magnetic refrigeration prototype using permanent magnets for operation, and a maximum temperature span 3.5 K without thermal load was achieved. Bahl et al. [21] designed and constructed a novel rotary magnetic refrigeration device, and a large temperature span of 18.9 K was obtained at a heat load of 200 W. Eriksen et al. [22] built and tested a rotary active magnetic regenerator prototype, and a temperature span of 10.2 K was measured in the prototype. Yu et al. [23] described exhaustively and classified all the magnetocaloric prototypes presented before 2010. In this review, the magnetocaloric devices are classified as the first and second generations of room temperature magnetic refrigerators. The first generation employs superconducting magnets and runs at low-frequency of operation. The second generation uses rotating permanent magnets allowed to reach higher frequencies of operation. Recently, Greco et al. [24] summarized the state of art of all the room temperature solid-state prototypes for cooling and heat pumps before 2019. In 2018, Johra et al. [25] built and investigated a prototype of an active magnetic regenerator and heat pump for building application, and the maximum operating frequency of 2 Hz and coefficient of performance of 5 are obtained at a temperature span of 25 K.

The optimal parametric design of room-temperature magnetic refrigerators, including the optimal design of the refrigeration cycle parameters, will be an important project towards commercialized development. Some studies have focused on the theoretical investigation of magnetic refrigeration cycles. For example, Diguet et al. numerically investigated the performance characteristics of the magnetic Brayton [26] and Ericsson [27] refrigeration cycles. Wu et al. [28] presented and optimized the model of the irreversible magnetic Stirling cryocooler using paramagnetic material as the working substance. Wang et al. [29] established the irreversible cycle model of magnetic Brayton refrigerators and the optimal performance parameters were obtained at the maximum coefficient of performance.

For thermal energy conversion devices, thermoeconomic performance analysis is a powerful and effective method that combines exergy with conventional concepts from engineering economics to evaluate and optimize the design parameter and performance of energy systems [30]. Sahraie et al. [31] performed and optimized the thermodynamic modeling of a two-stage irreversible heat pump. Lucia et al. [32] obtained the relationship between the thermoeconomic function and the entropy increase in an irreversible Stirling heat pump. Xu et al. [33] established an irreversible regenerative ferromagnetic Ericsson refrigeration cycle and optimized the thermoeconomic performance of the refrigeration cycle.

Note that Gd is a second-order material and almost without hysteresis. Gd-based alloys such as GdDy, GdEr, and GdTe exhibit magnetocaloric properties similar to Gd and can lower the Curie temperature. In this paper, an irreversible model of the regenerative magnetic Brayton refrigeration cycle using Gd, $Gd_{0.95}Dy_{0.05}$ or $Gd_{0.95}Er_{0.05}$ as the working substance is put forward. The influences of thermodynamic parameters including the adiabatic irreversibility factor, regenerator efficiency, heat leak coefficient, state point temperature of the working substance, and the area distribution of the heat exchanger in lower temperature side, and thermoeconomic parameter on the thermodynamic and thermoeconomic performances of the regeneration refrigeration cycle are analyzed and evaluated. At the same time, the impact of the investment cost of magnetic material in the refrigerator on the thermoeconomic performance is investigated. By using de Gennes factor method, the theoretical values of the Curie temperatures of these Gd-based alloys are calculated and compared with the related experimental data in Appendix. Furthermore, the comparisons of the thermoeconomic performance among $Gd_{0.95}Er_{0.05}$, $Gd_{0.95}Dy_{0.05}$, and Gd

are carried out by the numerical calculation results. The results obtained are helpful to the optimal parameter design and thermo-economic performance analysis for room temperature magnetic refrigerators.

2. Mathematical description of an irreversible magnetic Brayton refrigeration cycle

An irreversible magnetic Brayton refrigeration cycle consists of two *iso*-magnetic field and two adiabatic processes, as shown in Fig. 1. This refrigeration cycle is operated between the applied magnetic fields H_0 and H_1. The temperatures of cold and hot reservoirs are T_l and T_h, respectively. In the irreversible process a→ b', the working substance is magnetized adiabatically, and its temperature increases from T_h to $T_{b'}$ (T_b for a reversible process). In the *iso*-magnetic field process $b' \rightarrow c$, the heat Q_h is released from the working substance to the hot reservoir, such that the temperature of the working substance decreases from $T_{b'}$ to T_c, which is the temperature of the state point *c*. The process $c \rightarrow d$ is the *iso*-magnetic field one, the heat Q_r is released from the working substance to the regenerator, and the temperature of the working substance drops to T_l. In the adiabatic demagnetization process $d \rightarrow e'$ (e point for a reversible process), the temperature of the working substance is decreased further. In the *iso*-magnetic field process $e' \rightarrow$ f, the working substance absorbs the heat Q_l from the cooled space and the temperature of the working substance rises to T_f. At last, for the *iso*-magnetic field process f→ a, the regenerator releases the heat Q_r to the working substance and the temperature of the working substance rises to T_h [34].

In the low-temperature side, the heat exchange between the working substance and the cooled space can be expressed as

$$C(H_0, T)dT = U_l A_l (T_l - T)dt \tag{1}$$

From Fig. 1 and Eq. (1), one can obtain the heat exchange time between the working substance and the cooled space as

$$t_2 = \int_{T_{e'}}^{T_f} \frac{C(H_0, T)dT}{U_l A_l (T_l - T)} \tag{2}$$

Similarly, the heat exchange time t_1 between the working substance and the hot reservoir is given by

$$t_1 = \int_{T_c}^{T_{b'}} \frac{C(H_1, T)dT}{U_h A_h (T - T_h)} \tag{3}$$

According to statistical mechanics, the equation of state and magnetization entropy of ferromagnetic materials as the working substance are given by [35]

$$M = NgJB_J(y) \tag{4}$$

and

$$S_M(H, T) = R'\left[\ln\frac{\sinh\left(\frac{2J+1}{2J}y\right)}{\sinh\left(\frac{y}{2J}\right)} - yB(y)\right] \tag{5}$$

where $y = g\mu_0\mu_B J(H + \lambda' M)/k'T$ and the Brillouin function $B_J(x)$ is given by

$$B_J(y) = \frac{2J+1}{2J}\coth\left(\frac{2J+1}{2J}y\right) - \frac{1}{2J}\coth\left(\frac{1}{2J}y\right) \tag{6}$$

Based on Eq. (5), we can calculate the *iso*-field heat capacity by the following equation:

$$C_H = T\left(\frac{\partial S_M}{\partial T}\right)_H \tag{7}$$

Assuming that total heat exchange area A in high- and low-temperature sides is constant. Then, parameter $\beta = A_l/A$ is called as the area distribution of the heat exchanger in the low-temperature side, and $A_h = (1-\beta)A$ can be obtained. Further, we define irreversible adiabatic magnetization and demagnetization factors η_{mag} and η_{demag} as

$$\eta_{mag} = \frac{T_b - T_h}{T_{b'} - T_h} \tag{8}$$

and

$$\eta_{demag} = \frac{T_l - T_{e'}}{T_l - T_e} \tag{9}$$

For a reversible adiabatic process from H_0 to H_1, one has

$$S_M(H_0, T) = S_M(H_1, T + \Delta T_{ad}) \tag{10}$$

By using Eq. (10), T_b and T_e in the adiabatic processes a-b and d-e can be solved out.

Besides, it is supposed that the total time t_r spent in the two regenerative processes is proportional to that in the two heat exchange processes, i.e.,

$$t_r = \lambda(t_2 + t_1) \tag{11}$$

Note that λ depends on the property of the working substance. Thus, the period of the irreversible regeneration magnetic Brayton refrigeration cycle may be expressed as

$$\tau = (1 + \lambda)(t_2 + t_1) \tag{12}$$

In the regenerative magnetic Brayton refrigeration cycle model, it is designed that the heat released from the working substance to the regenerator is equal to that from the regenerator to the working substance, i.e., the regeneration quantity

$$Q_r = \int_{T_l}^{T_c} C(H_1, T)dT = \int_{T_f}^{T_h} C(H_0, T)dT \tag{13}$$

However, the regenerator is generally not perfect so that the additional regenerative loss ΔQ_r in the refrigeration system should be taken into account. It is reasonable to assume that the additional regenerative loss ΔQ_r is directly proportional to Q_r such that ΔQ_r may be expressed as [33]

$$\Delta Q_r = (1 - \eta)Q_r \tag{14}$$

On the other hand, the heat leak per cycle is also inevitable for an actual refrigerator. For this reason, we consider the heat leak loss between the hot reservoir and the cooled space in this refrigeration cycle model, which can be expressed as

$$Q_{leak} = U_{leak} A(T_h - T_l)\tau \tag{15}$$

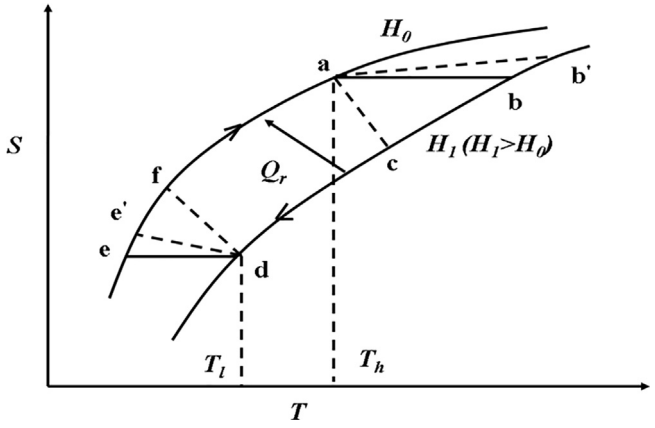

Fig. 1. The schematic diagram of an irreversible regeneration magnetic Brayton refrigeration cycle.

3. The thermodynamic and thermoeconomic functions of the refrigeration cycle

Based on the above refrigeration cycle model, one can obtain that the net cooling quantity Q_{net}, work input W, and cooling rate R are, respectively, given by

$$Q_{net} = \int_{T_{e'}}^{T_f} C(H_0, T)dT - (1-\eta)Q_r - U_{leak}A(T_h - T_l)\tau \tag{16}$$

$$W = Q_h - Q_l = \int_{T_c}^{T_{b'}} C(H_1, T)dT - \int_{T_{e'}}^{T_f} C(H_0, T)dT \tag{17}$$

and

$$R = \frac{Q_{net}}{\tau} = \frac{\int_{T_{e'}}^{T_f} C(H_0, T)dT - (1-\eta)Q_r}{(1+\lambda)\left[\int_{T_{e'}}^{T_f} \frac{C(H_0,T)dT}{U_l A_l (T_l - T)} + \int_{T_c}^{T_{b'}} \frac{C(H_1,T)}{U_h A_h (T - T_h)} dT\right]} - U_{leak} A(T_h - T_l) \tag{18}$$

Similarly, the power input and *COP* can be expressed as

$$P = \frac{W}{\tau} = \frac{\int_{T_c}^{T_{b'}} C(H_1, T)dT - \int_{T_{e'}}^{T_f} C(H_0, T)dT}{(1+\lambda)\left[\int_{T_{e'}}^{T_f} \frac{C(H_0,T)dT}{U_l A_l (T_l - T)} + \int_{T_c}^{T_{b'}} \frac{C(H_1,T)}{U_h A_h (T - T_h)} dT\right]} \tag{19}$$

and

$$COP = \frac{Q_{net}}{W} = \frac{\int_{T_{e'}}^{T_f} C(H_0, T)dT - (1-\eta)Q_r - U_{leak}A(T_h - T_l)\tau}{\int_{T_c}^{T_{b'}} C(H_1, T)dT - \int_{T_{e'}}^{T_f} C(H_0, T)dT} \tag{20}$$

In order to facilitate the calculation, the dimensionless cooling rate and dimensionless power input are written as

$$R^* = R \Big/ U_l A T_l = \frac{\int_{T_{e'}}^{T_f} C(H_0, T)dT - (1-\eta)Q_r}{T_l(1+\lambda)\left[\int_{T_{e'}}^{T_f} \frac{C(H_0,T)dT}{\beta(T_l - T)} + \int_{T_c}^{T_{b'}} \frac{C(H_1,T)}{r_{h/l}(1-\beta)(T - T_h)} dT\right]} - \frac{(T_h - T_l)}{T_l} I_{leak} \tag{21}$$

and

$$P^* = P \Big/ U_l A T_l = \frac{\int_{T_c}^{T_{b'}} C(H_1, T)dT - \int_{T_{e'}}^{T_f} C(H_0, T)dT}{T_l(1+\lambda)\left[\int_{T_{e'}}^{T_f} \frac{C(H_0,T)dT}{\beta(T_l - T)} + \int_{T_c}^{T_{b'}} \frac{C(H_1,T)}{r_{h/l}(1-\beta)(T - T_h)} dT\right]} \tag{22}$$

where $r_{h/l} = U_h/U_l$.

The thermoeconomic function [33,34] of an irreversible Brayton refrigeration cycle can be defined as the cooling rate per unit cost, which mainly includes the investment cost C_i and energy cost C_e, i.e.,

$$F = \frac{R}{C_e + C_i} \tag{23}$$

The investment cost of a conventional refrigerator depends on its scale and therefore is proportional to the total heat transfer area, i.e., $C_i = aA$. For a magnetic refrigerator, the price of magnetic material used as the working substance is unable to be ignored. For example, for the prototype machine using Gd as the working substance, the price of magnetic material Gd accounts for around 11% of the prototype machine. Moreover, the amount of magnetic refrigerants required in a magnetic refrigerator will range from 0.01 to 100 kg according to its scale [36]. For this reason, the investment cost of a magnetic refrigerator is defined as $C_i = a(1+u)A$, where u is the percentage of magnetic material's price in the machine. On the other hand, the energy cost is proportional to the power input, i.e. $C_e = bP$. Thus, Eq. (23) can be re-written as

$$F = \frac{R}{a(1+u)A + bP} \tag{24}$$

Then, the dimensionless thermoeconomic function bF can be expressed as

$$bF = \frac{R}{k(1+u)A + P} \tag{25}$$

where $k = a/b$. Combining Eq. (25) with Eqs. (18) and (19), we obtain the dimensionless thermoeconomic function as

$$bF = \frac{R}{k(1+u)A + P} = \frac{\int_{T_{e'}}^{T_f} C(H_0, T)dT - (1-\eta)Q_r - I_{leak}(T_h - T_l)(1+\lambda)}{k(1+u)(1+\lambda)\left[\int_{T_{e'}}^{T_f} \frac{C(H_0,T)dT}{\beta(T_l - T)} + \int_{T_c}^{T_{b'}} \frac{C(H_1,T)}{r_{h/l}(1-\beta)(T - T_h)} dT\right] \Big/ U_l + \int_{T_c}^{T_{b'}} C(H_1, T)dT - \int_{T_{e'}}^{T_f} C(H_0, T)dT} \tag{26}$$

Eq. (26) is an important equation, from which the optimal thermoeconomic performance can be analyzed and discussed. In fact, when the related parameters, including magnetic material parameters, are given, the dimensionless thermoeconomic function is mainly dependent on the distribution area β of the heat exchanger as well as the temperature T_f.

Substituting Eq. (26) into the extreme condition $(\partial bF/\partial\beta) = 0$, one can obtain that when $\beta = \beta_{opt}(T_f)$, the thermoeconomic function acquires its maximum value, Further, by substituting $\beta_{opt}(T_f)$ into Eq. (26) and Eqs. (20) to (22), the maximum dimensionless thermoeconomic function and the corresponding cooling rate, power input, and *COP* of the irreversible regeneration magnetic Brayton refrigeration cycle can be obtained. In the following section, the maximum thermoeconomic function and optimal thermodynamic performances based on actual magnetic materials will be analyzed and discussed in detail.

4. Results and discussion

Eqs. (21), (22), and (26) indicate clearly that the performance of the irreversible regenerative magnetic Brayton refrigeration cycle depends on the structure and operating parameters such as irreversible magnetization and demagnetization factors η_{mag} and η_{demag}, temperature T_f of state point f, and area distribution β of the heat exchanger in the low-temperature side, regenerator efficiency η, thermoeconomic parameter k, dimensionless heat leak coefficient I_{leak}, and so on. In order to evaluate the influences of these parameters on the thermoeconomic and thermodynamic performances of the refrigeration cycle, the numerical examples are presented in the following discussion based on magnetic refrigeration materials Gd, $Gd_{0.95}Dy_{0.05}$, and $Gd_{0.95}Er_{0.05}$, whose Curie temperatures are chosen as 293 K, 287.5 K and 284.7 K, respectively (see Appendix).

4.1. Numerical examples

Fig. 2 shows that the three-dimensional graphs of (a) dimensionless thermoeconomic function bF, (b) dimensionless cooling rate R^*, and (c) dimensionless power input P^* for the working substance Gd varying with T_f and β. As seen in Fig. 2(a) and (b), there exist optimal parameters β and T_f that maximize the dimensionless thermoeconomic function and cooling rate, respectively. Fig. 2(a) shows that the maximum bF occurs at $\beta = 0.7$ and $T_f = 279.4$ K and is equal to 2.78. Fig. 2(b) shows that when the parameters β and T_f equal 0.6 and 278.3 K, respectively, there yields a maximum R^* with 1.44×10^{-3}. Fig. 2(c) shows that the dimensionless power input P^* is a monotonously decreasing function of T_f, whereas there is an optimal

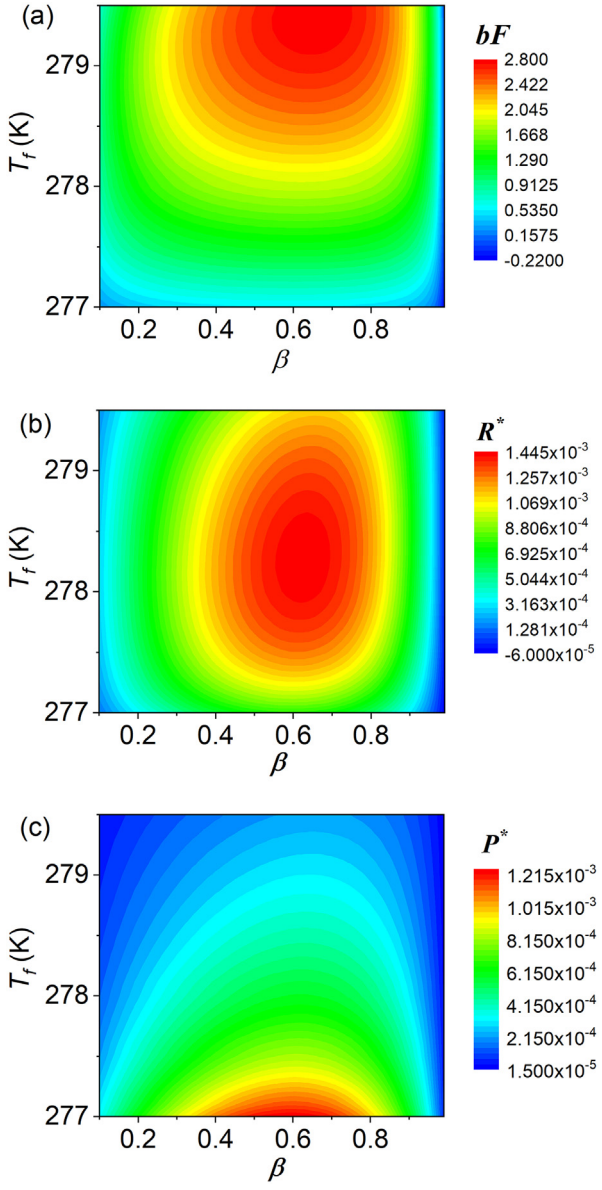

Fig. 2. The 3D graphs of (a) dimensionless thermoeconomic function bF, (b) dimensionless cooling rate, and (c) dimensionless power input with the working substance Gd versus β and T_f for T_l = 280 K, T_h = 295 K, $\mu_0 H_0$ = 0 T, $\mu_0 H_1$ = 2 T, $U_l = 1 \times 10^3 \mathrm{Wm^{-2}K^{-1}}$, $r_{h/l} = 2$, η_{mag} = 0.98, η_{demag} = 0.98, λ = 0.8, $k = 45 \mathrm{Wm^{-2}}$, u = 0.11, η = 0.96, and I_{leak} = 0.002.

parameter β that yields a maximum P^*.

The maximum dimensionless thermoeconomic function $b\mathrm{F}_{\max}$ and the corresponding optimal parameters β_{bF} and $T_{f,bF}$ for different working substances Gd, $\mathrm{Gd_{0.95}Dy_{0.05}}$, and $\mathrm{Gd_{0.95}Er_{0.05}}$ are listed in Table 1. The values of the maximal cooling rate $R^*_{\max}$ and the corresponding optimal β_R and $T_{f,R}$ for Gd,$\mathrm{Gd_{0.95}Dy_{0.05}}$, and $\mathrm{Gd_{0.95}Er_{0.05}}$ are also presented in Table 1. As seen from Table 1, both the dimensionless thermoeconomic function and the dimensionless cooling rate using Gd or $\mathrm{Gd_{0.95}Dy_{0.05}}$ as the working substance are better than those using $\mathrm{Gd_{0.95}Er_{0.05}}$ as the working substance.

4.2. The optimal thermoeconomic function bF_{opt} and the corresponding parameters

Fig. 3 shows that the optimal thermoeconomic function bF_{opt} and the corresponding dimensionless cooling rate $R^*_{bF,\beta}$, $COP_{bF,\beta}$, and power input $P^*_{bF,\beta}$ versus T_f curves, where β has been optimized. From Fig. 3, one can find that the dimensionless power input $P^*_{bF,\beta}$ and $COP_{bF,\beta}$ are, respectively, monotonically decreasing and increasing functions of T_f, while both bF_{opt} and $R^*_{bF,\beta}$ have their respective maxima for the different optimum values of the temperature T_f. For example, when T_f = 279.4 K, the optimal thermoeconomic function bF_{opt} attains its maximum 2.78. In such a case, $R^*_{bF,\beta}$ and $COP_{bF,\beta}$ are equal to around 1.17×10^{-3} and 0.24, respectively; when T_f = 278.3 K, the dimensionless cooling rate $R^*_{bF,\beta}$ attains its maximum 1.44×10^{-3}.

Fig. 4 shows the characteristic curves between the optimal thermoeconomic function bF_{opt} and the corresponding dimensionless cooling rate $R^*_{bF,\beta}$, between $R^*_{bF,\beta}$ and $COP_{bF,\beta}$, and between $b\mathrm{F}_{\mathrm{opt}}$ and $COP_{bF,\beta}$. It can be seen from Fig. 4(a) that for the three materials mentioned above, there is a negative slope region for the curves between bF_{opt} and $R^*_{bF,\beta}$. This implies that in the negative slope region, bF_{opt} decreases as R^*_{bF} increases, and it is an optimally working region for choosing suitable performance parameters bF_{opt} and $R^*_{bF,\beta}$. Because in the other regions, bF_{opt} or $R^*_{bF,\beta}$ has not reached its optimal value. Fig. 4(a) also indicates that when the other parameters of three materials are kept to be same values, the thermodynamic and thermoeconomic performances of Gd and $\mathrm{Gd_{0.95}Dy_{0.05}}$ are better than those of $\mathrm{Gd_{0.95}Er_{0.05}}$ in the optimal region. The maximum thermoeconomic function $bF_{,\max}$ of Gd is slightly larger than that of $\mathrm{Gd_{0.95}Dy_{0.05}}$, while $R^*_{bF,\max}$ of Gd is slightly smaller than that of $\mathrm{Gd_{0.95}Dy_{0.05}}$. Fig. 4(b) and (c) show that the $R^*_{bF,\beta}$ and bF_{opt} versus $COP_{bF,\beta}$ curves exhibit parabolic shape, and $R^*_{bF,\beta}$ and bF_{opt} have their respective maximum values, respectively. It is found once more from Fig. 4(b) and (c) that the thermodynamic and thermoeconomic performances using Gd or $\mathrm{Gd_{0.95}Dy_{0.05}}$ as the working substance are better than those using $\mathrm{Gd_{0.95}Er_{0.05}}$ as the working substance. For the sake of comparison, the values of the maximum thermoeconomic function $bF_{\ \max}$ and the corresponding dimensionless cooling rate R^*_{bF}, as well as the maximum value $R^*_{bF,max}$ of the optimal cooling rate $R^*_{bF,\beta}$ at the optimal thermoeconomic function $bF_{\ \mathrm{opt}}$ and the corresponding thermoeconomic function bF_{opt} are listed in Table 2.

Table 3 obtained from Eqs. (21) and (26) further indicates the effects of the percentage of magnetic material's price in the magnetic refrigerator on bF_{max}, bF_{opt}, and $R^*_{bF,\max}$ when Gd is used as the working substance. It can be found from Table 3 that bF_{max} and bF_{opt} decrease as u increases, whereas $R^*_{bF,\max}$ is independent of u. For other magnetic materials such as $\mathrm{Gd_{0.95}Dy_{0.05}}$ and $\mathrm{Gd_{0.95}Er_{0.05}}$, the similar calculation can be carried out based on Eqs. (21) and (26).

4.3. The effects of the relevant parameters on the maximum thermoeconomic function

Fig. 5 shows the curves of the maximal thermoeconomic function bF_{max} varying with (a) adiabatic magnetization factor η_{mag}, (b) adiabatic demagnetization factor η_{demag}, (c) thermoeconomic parameter k, (d) regenerator efficiency η, and (e) heat leak coefficient I_{leak}. As seen in Fig. 5(a) and (b), the maximal thermoeconomic function bF_{max} increases monotonously with increasing η_{mag} or η_{demag}, and the maximal thermoeconomic functions bF_{max} of Gd and $\mathrm{Gd_{0.95}Dy_{0.05}}$ are larger than that of $\mathrm{Gd_{0.95}Er_{0.05}}$ for a given η_{mag} or η_{demag}. The maximal thermoeconomic function bF_{max} of $\mathrm{Gd_{0.95}Dy_{0.05}}$ is higher than that of Gd when η_{mag} is smaller than 0.96. Fig. 5(c) shows that the maximal thermoeconomic function bF_{max} decreases monotonously as the thermoeconomic parameter k increases. The reason is that the cost of the

Table 1
The values of the maximum thermoeconomic function and cooling rate as well as the corresponding β and T_f for three different working substances.

Material	bF_{max}	β_{bF}	$T_{f,bF}$ (K)	$R^*_{\max}$	β_R	$T_{f,R}$ (K)
Gd	2.78	0.7	279.4	1.44×10^{-3}	0.6	278.3
$\mathrm{Gd_{0.95}Dy_{0.05}}$	2.75	0.5	278.7	1.44×10^{-3}	0.6	277.6
$\mathrm{Gd_{0.95}Er_{0.05}}$	2.52	0.5	277.8	1.37×10^{-3}	0.5	277.0

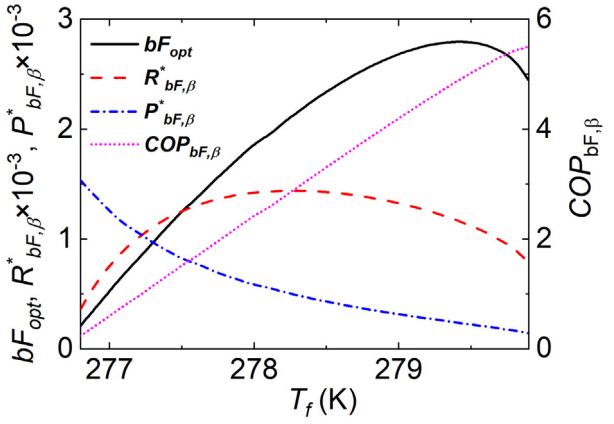

Fig. 3. The curves of the optimal thermoeconomic function bF_{opt}, the corresponding dimensionless cooling rate $R^*_{bF,\beta}$, dimensionless power input $P^*_{bF,\beta}$ and $COP_{bF,\beta}$ with the working substance Gd varying with T_f, where the values of other parameters are the same as those used in Fig. 2.

refrigeration system increases with the increase of the thermoeconomic parameter k, which must result in a decrease in bF_{max}. Fig. 5(d) and (e) show that the maximal thermoeconomic function bF_{max} monotonously increases as the regenerator efficiency η increases, but decreases with increasing heat leak coefficient I_{leak}. This may be explained as follows: because the dimensionless cooling rate R^* increases as the regenerator efficiencyη increases and heat leak coefficient I_{leak} decreases such that the thermoeconomic function bF increases. Moreover, from Fig. 5 one can find that the thermoeconomic performance using Gd as the working substance is generally better than that using $Gd_{0.95}Dy_{0.05}$ or $Gd_{0.95}Er_{0.05}$ as the working substance.

5. Conclusions

In the present paper, an irreversible regenerative magnetic Brayton refrigeration cycle model is established, in which the nonperfect regenerator, regenerative time, heat leak loss, irreversible adiabatic processes are taken into account. The mathematical expressions of the cooling rate, power input and thermoeconomic function of the irreversible regenerative refrigeration cycle are derived. The thermoeconomic function is used to evaluate and optimize the performances of the refrigeration cycle. Furthermore, by employing Gd, $Gd_{0.95}Dy_{0.05}$, or $Gd_{0.95}Er_{0.05}$ respectively as the working substance, the optimal value of the thermoeconomic function and the corresponding cooling rate are calculated and the values of the maximum thermoeconomic function and the corresponding optimal cooling rate are obtained. The influence of investment cost of the working substance on the thermoeconomic function is investigated. The impacts of the regenerator efficiency η, adiabatic magnetization/demagnetization factor η_{mag}/η_{demag}, heat leak coefficient I_{leak}, thermoeconomic parameter k on the thermoeconomic performance of the magnetic refrigeration cycles with three working substances are revealed. The results show that the thermoeconomic function increases with the increase of the adiabatic magnetization/demagnetization factor and regenerator efficiency, but decreases as the thermoeconomic parameter and heat leak coefficient increase. The regenerative Brayton refrigeration cycle using Gd or $Gd_{0.95}Dy_{0.05}$ as the working substance presents better thermoeconomic performance than that using $Gd_{0.95}Er_{0.05}$ as the working substance. Moreover, the thermoeconomic performance using $Gd_{0.95}Dy_{0.05}$ as the working substance is better than that using Gd as the working substance at the situation of lower adiabatic magnetization factor.

Declaration of Competing Interest

The authors declare that they have no known competing financial

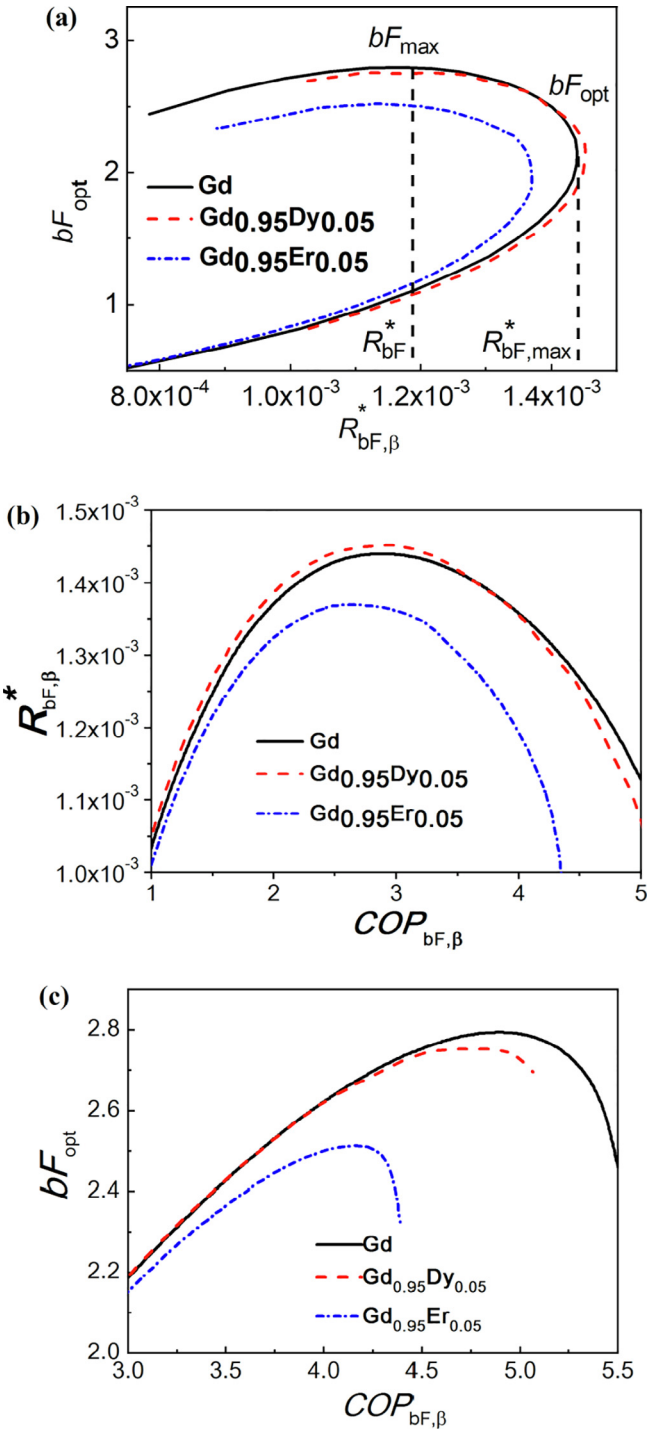

Fig. 4. Relationships of the optimal thermoeconomic function bF_{opt}, the corresponding dimensionless cooling rate $R^*_{bF,\beta}$ and $COP_{bF,\beta}$ for three working substances, where the related parameter values are the same as those used in Fig. 2.

Table 2
The values of the maximum thermoeconomic function bF_{max} and the corresponding R^*_{bF} as well as the maximum value $R^*_{bF,max}$ of $R^*_{bF,\beta}$ and the corresponding thermoeconomic function bF_{opt} for three working substances.

Material	bF_{max}	R^*_{bF}	$R^*_{bF,max}$	bF_{opt}
Gd	2.78	1.17×10^{-3}	1.44×10^{-3}	2.11
$Gd_{0.95}Dy_{0.05}$	2.75	1.11×10^{-3}	1.45×10^{-3}	2.20
$Gd_{0.95}Er_{0.05}$	2.52	1.14×10^{-3}	1.37×10^{-3}	1.97

Table 3
Effects of investment cost ratio of the working substance (Gd) on the thermo-economic performance.

u	$bF_{\max}$	$R^{*}_{bF,\max}$	bF_{opt}
0.05	2.82	1.44×10^{-3}	2.14
0.08	2.79	1.44×10^{-3}	2.12
0.11	2.78	1.44×10^{-3}	2.11
0.14	2.73	1.44×10^{-3}	2.10
0.17	2.70	1.44×10^{-3}	2.08

interests or personal relationships that could have appeared to influence the work reported in this paper.

Acknowledgment

This work has been supported by the National Natural Science Foundation of China (No. 51776178).

Appendix

Based on de Gennes factor model [37] and the data listed in Table 1A, the theoretical values of Curie temperatures T_C of $Gd_{1-x}R_x$(R = Dy, Er) can be calculated. Fig. 1A shows the theoretical and experimental values of Curie temperatures for $Gd_{1-x}R_x$(R = Dy, Er) versus R-doped content x curves. From Fig. 1A, it is found that the theoretical results are preferably consistent with the measured ones for Curie temperatures of Gd [38], $Gd_{0.88}Dy_{0.12}$ [39], $Gd_{0.8}Dy_{0.2}$ [40], $Gd_{0.73}Dy_{0.27}$ [41], $Gd_{0.6}Dy_{0.4}$ [42], $Gd_{0.5}Dy_{0.5}$ [41], $Gd_{0.9}Er_{0.1}$ [42], and $Gd_{0.84}Er_{0.16}$ [11]. It is also found that the difference between the theoretical and experimental data for Gd-Er samples increases as the Er concentration in Gd-Er alloy increases. In the text, Gd, $Gd_{0.95}Dy_{0.05}$, and $Gd_{0.95}Er_{0.05}$, whose Curie temperatures are 293 K, 287.5 K and 284.7 K, respectively, have been chosen as the working substances for some numerical examples to analyze thermodynamic and thermoeconomic performances of the magnetic Brayton refrigeration cycle.

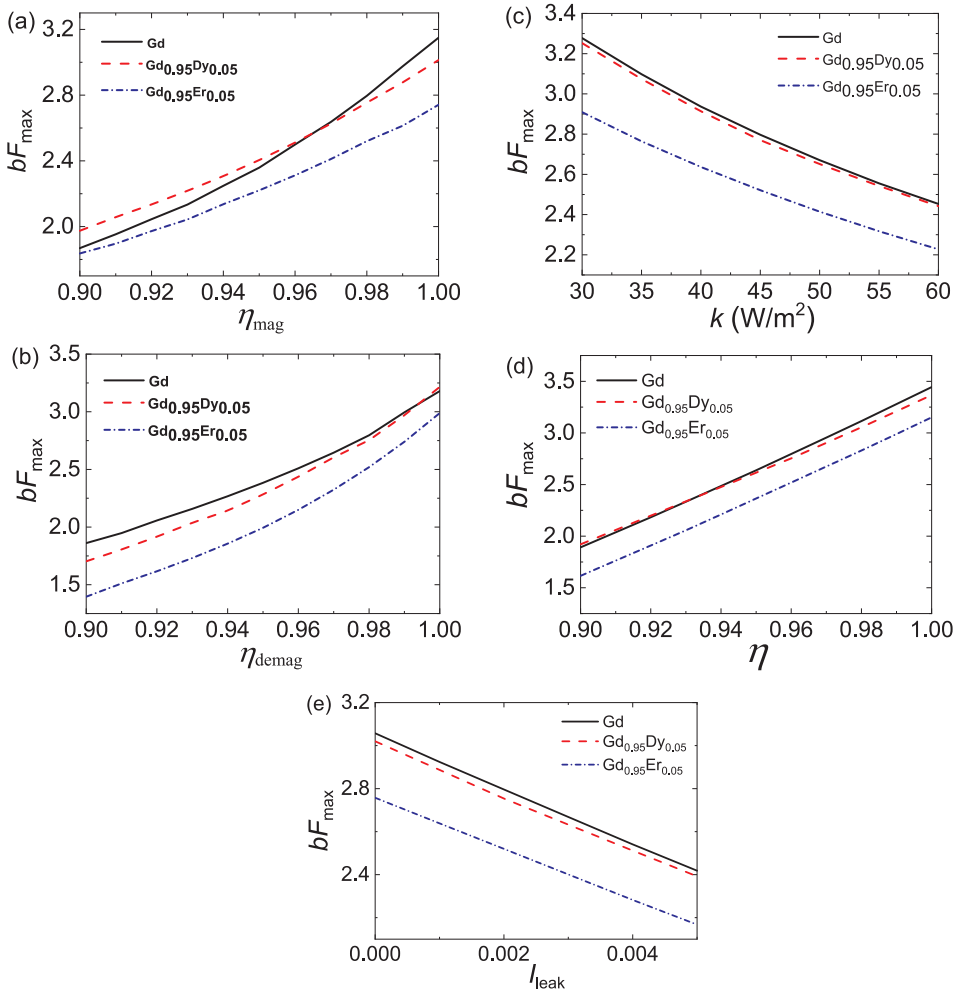

Fig. 5. The maximal thermoeconomic function bF_{max} versus (a) adiabatic magnetization factor η_{mag}, (b) adiabatic demagnetization factor η_{demag}, (c) thermoeconomic parameter k, (d) regenerator efficiency η, and (e) dimensionless heat leak coefficient I_{leak} curves.

Table 1A
The related parameter values of Gd, Dy, Er [37,43–45].

Material	Lander factor g	Angular quantum number J	Debye temperature T_D(K)	Molar mass M_m(kg/mol)	Density ρ(kg/m^3)
Gd	2	3.5	173	0.157	7901
Dy	1.33	7.5	180	0.1625	8540
Er	1.2	7.5	230	0.167	9066

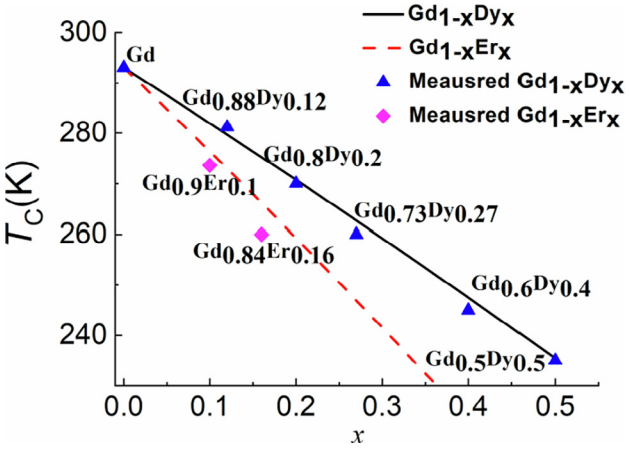

Fig. 1A. The theoretical and measured Curie temperatures of $Gd_{1-x}R_x$(R = Dy, Er) versus R-doped content x.

References

[1] K.A. Gschneidner Jr, V.K. Pecharsky, A.O. Tsokol, Rep. Prog. Phys. 68 (2005) 1479–1539.
[2] E. Brück, O. Tegus, D.T.C. Thanh, K.H.J. Buschow, J. Magn, Magn. Mater. 310 (2007) 2793–2799.
[3] M.H. Phan, S.C. Yu, J. Magn, Magn. Mater. 308 (2007) 325–340.
[4] A. Kitanovski, P.W. Egolf, Int. J. Refrig. 29 (2006) 3–21.
[5] H. Zhang, R. Gimaev, B. Kovalev, K. Kamilov, V. Zverev, A. Tishin, Phys. B 558 (2019) 65–73.
[6] B. Monfared, B. Palm, Int. J. Refrig. 96 (2018) 25–37.
[7] Z.G. Zheng, D.C. Zeng, Z.G. Qiu, J. Magn. Magn. Mater., 465 (2018) pp. 19–24.
[8] G. Diguet, G.X. Lin, J.C. Chen, J. Magn. Magn. Mater. 326 (2013) 103–107.
[9] J.R. Gómez, R.F. Garcia, A. Catoira, M.R. Gómez, Renew. Sust. Energy Rev. 17 (2013) 74–82.
[10] A. Smaili, R. Chahine, Advances in Cryogenic Engineering Materials, Springer, Boston, MA, 1996, pp. 445–450.
[11] A.M. Tishin, Cryogenics 30 (1990) 720–725.
[12] Y.S. Koshkid'ko, J. Ćwik, T.I. Ivanova, S.A. Nikitin, M. Miller, K. Rogacki, J. Magn. Magn. Mater. 433 (2017) 234–238.
[13] A.P. Kamantsev, V.V. Koledov, A.V. Mashirov, E.T. Dilmieva, V.G. Shavrov, J. Cwik, A.S. Los, V.I. Nizhankovskii, K. Rogacki, I.S. Tereshina, Y.S. Koshkid'ko, M.V. Lyange, V.V. Khovaylo, P. Ari-Gur, J. Appl. Phys. 117 (2015) 163903.
[14] V.K. Pecharsky, K.A. Gschneidner Jr., Phys. Rev. Lett. 78 (1997) 4494.
[15] C. Aprea, A. Greco, A. Maiorino, C. Masselli, Therm. Sci. Eng. Prog. 6 (2018) 370–379.
[16] A. Waske, M.E. Gruner, T. Gottschall, O. Gutfleisch, MRS Bull. 43 (2018) 269–273.
[17] V. Franco, J.S. Blázquez, J.J. Ipus, J.Y. Law, L.M. Moreno-Ramírez, A. Conde, Prog. Mater. Sci. 93 (2018) 112–232.
[18] T. Samanta, I. Das, S. Banerjee, Appl. Phys. Lett. 91 (2007) 152506.
[19] Z.B. Guo, Y.W. Du, J.S. Zhu, H. Huang, W.P. Ding, D. Feng, Phys. Rev. Lett. 78 (1997) 1142.
[20] J.R. Gómez, R.F. Garcia, J.C. Carril, M.R. Gómez, Int. J. Refrig. 36 (2013) 1388–1398.
[21] C.R.H. Bahl, K. Engelbrecht, D. Eriksen, J. Lozano, R. Bjørk, J. Geyti, K.K. Nielsen, A. Smith, N. Pryds, Int. J. Refrig. 37 (2014) 78–83.
[22] D. Eriksen, K. Engelbrecht, C.R.H. Bahl, R. Bjørk, Int. J. Refrig. 58 (2015) 14–21.
[23] B. Yu, M. Liu, P.W. Egolf, A. Kitanovski, Int. J. Refrig. 33 (2010) 1029–1060.
[24] A. Greco, C. Aprea, A. Maiorino, C. Masselli, Int. J. Refrig. 106 (2019) 66–88.
[25] H. Johra, K. Filonenko, P. Heiselberg, C. Veje, S. Dall'Olio, K. Engelbrecht, C. Bahl, Renew. Energy 136 (2019) 115–126.
[26] G. Diguet, G.X. Lin, J.C. Chen, Int. J. Refrig. 35 (2012) 1035–1042.
[27] G. Diguet, G.X. Lin, J.C. Chen, J. Magn, Magn. Mater. 350 (2014) 50–54.
[28] F. Wu, L.G. Chen, C.H. Wu, F.R. Sun, Y.H. Zhu, Int. J. Eng. Sci. 39 (2001) 361–368.
[29] H. Wang, S.Q. Liu, Phys. Scr. 77 (2008) 065702.
[30] G. Tsatsaronis, Progr. Energy Combust. Sci. 19 (1993) 227–257.
[31] H. Sahraie, M.R. Mirani, M.H. Ahmadi, M. Ashouri, Energy Convers. Manage. 99 (2015) 81–91.
[32] U. Lucia, G. Gervino, Eur. Phys. J. B 50 (2006) 367–369.
[33] Z.C. Xu, J.C. Guo, G.X. Lin, J.C. Chen, J. Magn, Magn. Mater. 409 (2016) 71–79.
[34] H. Wang, G.X. Wu, Sci. China Phys. Mech. 55 (2012) 187–194.
[35] R. Pathria, Statistical Mechanics, Pergamon Press Ltd., Oxford, 1972.
[36] K.A. Gschneidner Jr, V.K. Pecharsky, J. Rare Earths 24 (2006) 641–647.
[37] C. Aprea, A. Greco, A. Maiorino, Energy Convers. Manage. 70 (2013) 40–55.
[38] J.W. Cable, E.O. Wollan, Phys. Rev. 165 (1968) 733–734.
[39] A. Smaïli, R. Chahine, J. Appl. Phys. 81 (1997) 824–829.
[40] X.L. Hou, S.T. Li, A. Zhang, H. Xu, J.S. Ni, B.X. Zhou, Phys. Stat. Sol. 4 (2007) 4564–4568.
[41] W. Dai, B.G. Shen, D.X. Li, Z.X. Gao, J. Alloys Compd. 311 (2000) 22–25.
[42] A. Smaïli, R. Chahine, Adv. Cryog. Eng. 42 (1996) 445–450.
[43] A. Smaïli, R. Chahine, Cryogenics 38 (1998) 247–252.
[44] N.A. de Oliveira, P.J. von Ranke, Phys. Rep. 489 (2010) 89–159.
[45] K.H.J.Buschow, F.de Boer, Kluwer Academic Publishers, NewYork, 2003.